Title: **Addition Reaction of Alkyl Radical to the C_{60} Fullerene: Density Functional Theory (DFT) Study**

Authors: Hiroto TACHIKAWA* and Hiroshi KAWABATA

Division of Applied Chemistry, Graduate School of Engineering,
Hokkaido University, Sapporo 060-8628, JAPAN

Manuscript submitted to : *JJAP*

Section of the journal : Special Issue [EM-NANO]

Running Title : Alkyl functionalized fullerene

Correspondence and Proof to : Dr. Hiroto TACHIKAWA*
Division of Applied Chemistry
Graduate School of Engineering
Hokkaido University
Sapporo 060-8628, JAPAN
hiroto@eng.hokudai.ac.jp
Fax. +81 11706-7897

Contents :

2015_09_01 revised

Addition Reaction of Alkyl Radical to the C_{60} Fullerene: Density Functional Theory (DFT) Study

Hiroto TACHIKAWA* and Hiroshi KAWABATA

Department of Applied Chemistry, Graduate School of Engineering, Hokkaido University, Sapporo 060-8628, JAPAN

Abstract: Functionalized fullerenes are known as a high-performance molecule. In this study, the alkyl-functionalized fullerenes (denoted by R-C_{60}) have been investigated by means of density functional theory (DFT) method to elucidate the effects of functionalization on the electronic states of fullerene. Also, the reaction mechanism of alkyl radical with C_{60} was investigated. The methyl, ethyl, propyl and butyl radicals (denoted by *n*=1-4, where ***n*** means number of carbon atoms in alkyl radical) were examined as alkyl radicals. The DFT calculation showed that the alkyl radical binds to the carbon atom of C_{60} in the on-top site, and a strong C-C single bond was formed. The binding energies of alkyl radicals to C_{60} were distributed in the ranges 31.8-35.1 kcal mol^{-1} at the CAM-B3LYP/6-311G(d,p) level. It was found that the activation barrier exists before the alkyl addition: the barrier heights were calculated to be 2.1-2.8 kcal mol^{-1}. The electronic states of R-C_{60} complex were discussed on the basis of theoretical results.

KEYWORDS: radical addition; spin density; potential energy curve; absorption spectrum; hyperfine coupling constant

Corresponding author: Hiroto TACHIKAWA, FAX: +81-11-706-7897

E-mail: hiroto@eng.hokudai.ac.jp

1. Introduction

Functionalized fullerenes are known as a high-performance molecule. For example, methanofullerene ([6,6]-phenyl-C_{61}-butyric acid methyl ester: PCBM) is one of the most useful *n*-type organic semiconductors [1-7]. The interaction between organic radical and fullerene has recently attracted considerable interest because the electronic properties of carbon materials are drastically changed by the addition of radical [8-15]. Alkyl radical (C_nH_{2n+1}) is the simplest organic radical and is sometimes utilized in the surface modification of carbon materials such as diamond [16], graphene, and fullerene [17]. The radical influences strongly electronic conductivity and the band gap in the semi-conductor. Also, the fullerene and graphene materials have a possibility as a radical storage medium. Therefore, the elucidation of an electronic state and the formation mechanism of radical added carbon materials are an important theme to develop the high performance materials.

The interaction of hydrogen atom with fullerenes has been investigated as radical added fullerenes. Using density functional theory (DFT) calculations, Tokunaga et al. have investigated electronic states of mono- and di-hydrated fullerene, $C_{60}H$ and $C_{60}H_2$. [18] They found that energy of $C_{60}H$ radical is smaller than the summation of energy of the fullerene and that of hydrogen atom. They also calculated cationic states of $C_{60}H$, $C_{60}H^+$, and found that dipole moment of $C_{60}H$ becomes significantly larger in cationic state.

In case of graphene-hydrogen atom system, Novoselov and co-workers showed experimentally that the electronic property of graphene is drastically changed: the highly conductive graphene is converted from a semimetal into an insulator [19]. The reaction with hydrogen was reversible.

Raman studies revealed that the hydrogenation interrupts the delocalized π-bonding system of graphene through the formation of sp^3 carbon–hydrogen bonds [20]. From the transmission electron microscopy, it was found that the hydrogenation is reversible through annealing, thereby restoring the conductivity and structure of graphene. This reversibility also creates the possibility of hydrogen storage.

The interaction between graphene surface and hydrogen atom have been investigated by means of DFT calculation. [21-26] Casolo et al. investigated the adsorption of hydrogen atom to a 5x5 surface unit cell of graphene using the DFT method [21]. The binding energies per one hydrogen atom were calculated in the range 0.8-1.9 eV and a barrier to sticking in the range 0-0.15 eV. It was suggested that the change of hybrid orbital from sp^2 to sp^3 is important in the addition of H atom to graphene. Thus, the electronic states of H atom on graphene and C_{60} surfaces are understood theoretically. However, interaction of organic radical with C_{60} is not clearly understood. Especially, the addition process of alkyl radicals to C_{60} surface is scarcely known.

In the present study, the addition reaction of simple alkyl radicals (R) to the C_{60} surface was investigated by means of DFT method. We focus our attention mainly on the mechanism of addition process of alkyl radical to the C_{60} surface. We have searched the transition state structure of radical addition to the C_{60} surface. Also, potential energy curve of alkyl radical approaching to the surface was investigated.

2. Method of calculation

All DFT calculations were carried out using Gaussian 09 program package.[15] The geometries of free C_{60} and complexes of C_{60} with alkyl radical (R) (expressed by R-C_{60}), were fully optimized at the CAM-B3LYP/6-31G(d) and CAM-B3LYP/6-311G(d,p)

levels. Previous works showed that these levels of theory give reasonable electronic structures of graphene systems [28-30]. To confirm the stabilities of molecules at the stationary points along the reaction coordinate, the harmonic vibrational frequencies were calculated at the CAM-B3LYP/6-31G(d) level. The barrier height at the transition state and binding energy were also calculated at the CAM-B3LYP/6-311G(d,p) level. Potential energy curve for the approach of alkyl radical to C_{60} were calculated at the CAM-B3LYP/6-31G(d) level. The electronic states of R-C_{60} were obtained by natural population analysis and natural bond orbital (NBO) methods at the CAM-B3LYP/6-311G(d,p) level. The binding energy of alkyl radical to C_{60}, E_{bind} (n), is defined by

$$E_{bind}\,(n) = \quad E_{R(n)\text{-}C60} - \quad [E_{R(n)} + E(C_{60})].$$

where, $E_{R(n)\text{-}C60}$ means total energy of the R-C_{60} complex with ***n***. $E_{R(n)}$ and $E(C_{60})$ are total energies of alkyl radical and C_{60}, respectively.

3. Results

3.1 Binding structures

The optimized structures of the R-C_{60} system are illustrated in Figure 1. We discuss the structures and electronic states of R-C_{60} using the results of the most sophisticated calculation (CAM-B3LYP/6-311G(d,p) level). In case of n=4 (butyl radical), two conformers exist as structural form: normal butyl (4n) and tertiary butyl (4t) radicals. The calculations showed that all alkyl radicals can bind to the on-top site of C_{60}.

In case of ethyl radical (n=2, C_2H_5), the C_0-C_1 bond distance was calculated to be R_1=1.554 Å, which was slightly longer than that of methyl radical (1.543 Å, n=1). The planar structure of methylene moiety of ethyl radical was changed to a bent form after the binding to the C_{60} surface. The bending angle was calculated to be θ_1 =<C_0-C_1-C_2 =

114.9°. The C_1-H bond distance was 1.093 Å, which was slightly elongated from that of free ethyl radical (1.082 Å). The C_0-C_1 bond distances were almost constant in *n*=2, 3, and 4n (~1.554 Å). On the other hand, the distance in n=4t (1.588 Å) was longer than those of n=1-4n (~1.554 Å). This elongation was due to the steric hindrance between methyl group of 4t and C_{60} surface.

The binding energies of alkyl radicals to C_{60} (E_{bind}) are given in Table 1. The binding energies of R for *n*=1, 2, 3, 4n, and 4t were calculated to be +35.1, +31.8, +32.2, +32.1, and +24.1 kcal mol^{-1}, respectively, indicating that the binding energy decreases with increasing ***n***. The binding energy for n=4t was significantly smaller than that of n=4 (24.1 vs. 32.1 kcal mol^{-1}). This is due to the steric hindrance of methyl groups in tertiary butyl radical. The similar results were obtained from the CAM-B3LYP/6-31G(d) calculations. The NPA charges on moieties of C_{60} and R were -0.1 and +0.1, respectively. These values indicate that the alkyl part behaves as a slight electron donor in R-C_{60}. The result indicates that an electron transfer takes place from alkyl radical to C_{60} after the addition: $R + C_{60} \rightarrow (R)^{\delta+} (C_{60})^{\delta-}$.

The van der Waals (vdW) structures of R--C_{60} were obtained at the entrance region in the binding reaction of R to C_{60}. The optimized distances between C_0 and C_1 are given in Table 2 together with the binding energies of vdW (E_{vdW}). The distances of alkyl radicals from C_{60} surface were calculated to be 3.56-3.68 Å. The structures of alkyl radicals were close to those of free alkyl radicals.

3.2. Potential energy curve (PEC)

Potential energy curve (PEC) for the approach of butyl radical (n=4n) to the C_{60} surface is plotted in Figure 2 as a function of C_0-C_1 distance (r_1). All geometrical

parameters of the R-C_{60} system except for r_1 were optimized at each point of r_1.

When the butyl radical approaches to the C_{60} surface, the first energy minimum was found at r_1=r(C_0- C_1)=3.636 Å. This is due to a vdW complex composed of R and C_{60}. After that, the energy barrier was found at r_1=2.438 Å. This point corresponds to a transition state of R addition to C_{60}. The barrier height of TS was calculated to be 2.10 kcal mol^{-1} at the CAM-B3LYP/6-311G(d,p) level. The potential energy decreased significantly after TS and it reaches the lowest energy point corresponding to a bound state of R-C_{60} radical (PD).

3.3 Structures of transition state

The transition state (TS) structures of R--C_{60} are given in Figure 3. In the transition state of methyl radical addition, the distance of CH_3 from the surface was r_1=r(C_0-CH_3) = 2.424 Å, and the angle of C_0-C-H was θ_1=97.9°. An imaginary frequency corresponding to the CH_3 dissociation coordinate was detected by the vibrational analysis. The value was calculated to be 302 ***i*** cm^{-1}. This indicates that the structure of TS in fig. 3 corresponds to the true transition state and saddle point for the CH_3 dissociation and addition reactions. In alkyl radical additions of n=2-4, the distances (r_1) were 2.439, 2.437, and 2.438 Å, respectively. Also, the angles (θ_1) were 106.7° (n=2), 106.4° (n=3), and 107.2° (n=4). These results indicate that the structures in TS are very similar to each other. This is due to the fact that the interaction of alkyl radical with C_{60} is localized in 2p-orbital of alkyl radical. The chain part of alkyl radical behaves as a spectator in the alkyl radical addition.

The activation energies for the radical addition reaction are given in Table 3. The barrier heights of TS from the dissociation limit (C_{60} + R) were 2.8 kcal mol^{-1} (n=1) and

2.1 kcal mol^{-1} (n=2-4n), indicating that the activation energy is saturated in n=2-3. This is caused by the similarity of the TS structure in n=2-4.

3.4 Spin density along the reaction coordinate

The spatial distributions of spin density along the reaction coordinate are given in Figure 4. The spin density was only localized in the alkyl radical at longer separation, r(C_0-C)=3.636Å (vdW state). Especially, the unpaired electron was maily localized in the 2p orbital of the carbon atom of butyl radical (C_1). The spin density on the butyl radical was calculated to be 0.992. At the TS position, the spin was widely distributed around R and a part of the C_{60} surface. The spin density on R was 0.832.

At the binding structure (PD), i.e., the optimized structure of the R-C_{60} system, the spin density was fully distributed around the C_{60} surface. The spin density on R was changed to 0.04. This result indicates that the unpaired electron on alkyl radical (spin density) is fully transferred to the C_{60} surface by the radical addition.

3.5 Electronic states of alkyl functionalized fullerenes

The electronic states of carbon atom in the binding site (C_0) will be changed by the addition of alkyl radical. To elucidate the electronic state of the C_0 atom, the natural bond orbital (NBO) analysis was carried out for the R-C_{60} system. The NBO of the C_0-C_1 bond of free C_{60} was expressed by

$$\sigma_{C=C} = 0.707(sp^{2.15})_{C0} + 0.707(sp^{2.15})_{C5} \qquad (1)$$

where, C_0 and C_5 mean the carbon atom in addition center and neighbor positioned carbon atom, respectively. After the alkyl radical addition to C_{60}, the NBO was changed to be

$$\sigma_{C=C} = a(sp^m)_{C0} + b(sp^l)_{C1} \quad (2)$$

The values of ***m*** and ***l*** obtained by NBO analysis are given in Table 4. Before the addition, the carbon atom in the addition site (C_0) has a hybrid orbital composed of sp^2-type. After the addition of R, the configuration was changed from $sp^{2.15}$ to $sp^{3.0}$. This value indicates that the carbon atom (C_0) is changed from sp^2 to sp^3 hybrid orbitals after the radical addition.

3.6 Hyperfine coupling constants of R-C_{60}

Hyperfine coupling constant (hfcc) of radical species provides important information on the electronic states and structure of radical. In the present study, proton-hfccs of free alkyl radicals and R-C_{60} (n=1-4) were calculated at the CAM-B3LYP/6-311G(d,p) level. The results are given in Table 5. In case of free alkyl radicals, hfccs of α- and β-protons (denoted by H_1 and H_2, respectively) were significantly larger than the others. This result indicates that the unpaired electron was localized on C_1 and C_2 carbon atoms of free radical.

In vdW state, the hfccs were slightly decreased: for example, the hfccs of H_1 in R-C_{60} (n=4) were changed from -22.13 G (free radical) to -21.91 G (vdW). At the transition state (TS), the value of H_1 was further decreased to -16.44 G. The change was caused by the dissipation of unpaired electron from the alkyl radical to C_{60}. In final state (PD formation), the hfccs of H_1 and H_2 were close to zero (-0.97G and -0.08G, respectively). This result indicates that almost all unpaired electron is transferred from the radical to C_{60}. These significant changes suggest that the alkyl radical addition to C_{60} takes place together with the transfer of unpaired electron.

3.7 Absorption spectra of alkyl functionalized C_{60} fullerenes

Simulated absorption spectra of C_{60} and R-C_{60} are given in Figure 5. The C_{60} molecule showed a very weak peak: the absorption maximum was peaked at 4.50 eV. In vdW state, the peak was red-shifted to 3.83 eV, and the intensity of peak was about 100 times larger than that of C_{60}. The product CH_3-C_{60} has two peaks at 2.13 and 3.50 eV.

To assign the peaks appearing at low- and high-energy regions in CH_3-C_{60}, the molecular orbitals (MOs) contributing to the electronic excitations were analyzed. Three MOs were illustrated in Figure 6. The MOs contributing to the lower excitation were 182 and 185: the excitation from 182 to 185 shows the peak (c), where 182 and 185 are orbital numbers in CH_3-C_{60}. HOMO and LUMO correspond to 184 and 185, respectively. The excitation from 178 to 185 contributes to the peak (d). These results indicate that both electronic excitation bands (peaks c and d) are composed of charge transfer (CT) bands from C_{60} from CH_3 moiety of CH_3-C_{60}.

3.8 Potential energy diagram for the reaction

As a summary of the present study, potential energy diagrams of alkyl radical addition reaction to C_{60} surface is illustrated in Figure 7. The values indicate relative energies (in kcal mol^{-1}) along the reaction coordinate, and the zero level means total energy of C_{60} plus alkyl radical (RC). In the entrance region of the reaction, a weakly bound complex exists as a vdW complex. Before the addition to C_{60}, there is a transition state barrier. However, the barrier heights are very low (about 2.1 kcal mol^{-1}). The alkyl radicals were strongly bound to the C_{60} surface with the binding energy of ~35 kcal mol^{-1}.

4. Conclusion

The present calculations can be summarized as follows: (1) the alkyl radicals can react with a C_{60} surface and binds directly to the carbon atom (C_0), and C_0-C_1 strong single bond is formed. The binding energies of alkyl radical to C_{60} surface were calculated to be 31.8-35.1 kcal mol^{-1} at the CAM-B3LYP/6-311G(d,p) level. (2) Low activation barrier exists in the approach of alkyl radical to the C_{60} surface. This barrier was caused by a re-organization from sp^2 to sp^3 hybridization of carbon atom in the binding site (C_0 atom). The barrier heights were 2.1-2.8 kcal mol^{-1} at the CAM-B3LYP/6-311G(d,p) level, and (3) the spin density of alkyl radical is widely distributed over the C_{60} surface after the binding.

Acknowledgment. The author acknowledges partial support from JSPS KAKENHI Grant Number 15K05371 and MEXT KAKENHI Grant Number 25108004.

References

[1] Yu, HP.; Luo, H.; Liu, TT.; Jing, GY., Modern Phys. Lett. B., 29, 1550028 (2015)

[2]Devynck, M.; Rostirolla, B.; Watson, CP.; Taylor, DM.,Appl. Phys. Lett., 105,183301 (2014).

[3] F. Gajdos, H. Oberhofer, M. Dupuis, J. Blumberger, J. Phys. Chem. Lett. 4, 1012 (2013).

[4] I. Borges, Jr., A.J.A. Aquino, A. Köhn, R. Nieman, W.L. Hase, L.X. Chen, and H. Lischka, J. Am. Chem. Soc. 135, 18252 (2013).

[5] Armbruster, O.; Lungenschmied, C.; Bauer, S., Phys. Rev. B. 86, 235201 (2012).

[6] Armbruster, O.; Lungenschmied, C.; Bauer, S., Phys. Rev. B. 84, 085208 (2011).

[7] Watanabe, S.; Tanaka, H.; Ito, H.; Marumoto, K.; Kuroda, S., Synth. Metal. 159,893-896 (2009).

[8] B. Narayanan, Y. Zhao, C.V. Ciobanu, Appl. Phys. Lett., 100, 203901 (2012).

[9] V. Jimenez, A. Ramirez-Lucas, P. Sanchez, J.L. Valverde, A. Romero, Int. J. Hydrogen Energy, 37, 4144 (2012).

[10] V. Jimenez, A. Ramirez-Lucas, P. Sanchez, J.L. Valverde, A. Romero, Appl. Surf. Sci., 258, 2498 (2012).

[11] Mukai, K.; Shiba, D.; Mukai, K.; Yoshida, K.; Hisatou, H.; Ohara, K.; Hosokoshi, Y.; Azuma, N., Polyhedron, 24,2513-2521 (2005)

[12] Liu, TX.; Zhang, ZB.; Liu, QF.; Zhang, PL.; Jia, PH.; Zhang, ZG.; Zhang, GS., Org. Lett., 16, 1020-1023 (2014).

[13] Sabirov, D.S.; Garipova, R.R.; Bulgakov, R.G., J. Phys. Chem.A.117, 13176-13183 (2013).

[14] Bulgakov, R.G.; Galimov, D.I.; Gazeeva, D.R., Fuller. Nanotub. Car. N., 21, 869-878 (2013).

[15] Yumagulova, RK.; Medvedeva, NA.; Yakupova, LR.; Kolesov, SV.; Safiullin, RL., Kinet. Catal. 54,709-715 (2013)

[16] A.R. Sobia, S. Adnan, A. Mukhtiar, A.A. Khurram, A.A. Turab, A. Awais, A. Naveed, Q.J. Faisal, H. Javaid, G.J.Yu, Curr. Appl. Phys., 12, 712 (2012).

[17] S. Riahi, P. Pourhossein, A. Zolfaghari, MR. Ganjali, H.Z. Jooya, Fullerene Nanotube Carbon Nanostruct. 17, 159 (2009).

[18] K. Tokunaga, S. Ohmori, H. Kawabata, K. Matsushige, Jpn. J. Appl. Phys. 47, 1089 (2008).

[19] D.C. Elias, R.R. Nair, T.M.G. Mohiuddin, S.V. Morozov, P. Blake, M.P. Halsall, A.C. Ferrari, D.W. Boukhvalov, M.I. Katsnelson, A.K. Geim, and K.S. Novoselov, Science, 323, 610 (2009).

[20] M. Batzill, Surf. Sci. Rep. 67, 83 (2012).

[21] S. Casolo, O.M. Lowik, R. Martinazzo, and G.F. Tantardini: J. Chem. Phys. 130, 054704 (2009).

[22] R. H. Miwa, T.B. Martins, and A. Fazzio: Nanotechnology 19, 155708 (2008).

[23] P. Zhou, R. Lee, A. Claye, and J.E. Fischer: Carbon 36, 1777 (1998).

[24] T. Saito, K. Nomura, K. Mizoguchi, K. Mizuno, K. Kume, and H. Suematsu: J. Phys. Soc. Jpn. 58, 269 (1989).

[25] A. Ito, H. Nakamura, and A. Takayama: J. Phys. Soc. Jpn. 77, 114602 (2008).

[26] H. Tachikawa and T. Iyama, Jpn. J. Appl. Phys., 49, 06GJ12 (2010).

[27] Ab-initio calculation program: Gaussian 09, Revision B.04, M. J. Frisch, G. W. Trucks, H. B. Schlegel, G. E. Scuseria, M. A. Robb, J. R. Cheeseman, J. A. Montgomery,

Jr., T. Vreven, K. N. Kudin, J. C. Burant, J. M. Millam, S. S. Iyengar, J. Tomasi, V. Barone, B. Mennucci, MCossi, G. Scalmani, N. Rega, G. A. Petersson, H. Nakatsuji, M. Hada, M. Ehara, K. Toyota, R. Fukuda, J. Hasegawa, M. Ishida, T. Nakajima, Y. Honda, O. Kitao, H. Nakai, M. Klene, X. Li, J. E. Knox, H. P. Hratchian, J. B. Cross, C. Adamo, J. Jaramillo, R. Gomperts, R. E. Stratmann, O. Yazyev, A. J. Austin, R. Cammi, C. Pomelli, J. W. Ochterski, P. Y. Ayala, K. Morokuma, G. A. Voth, P. Salvador, J. J. Dannenberg, V. G. Zakrzewski, S. Dapprich, A. D. Daniels, M. C. Strain, O. Farkas, D. K. Malick, A. D. Rabuck, K. Raghavachari, J. B. Foresman, J. V. Ortiz, Q. Cui, A. G. Baboul, S. Clifford, J. Cioslowski, B. B. Stefanov, G. Liu, A. Liashenko, P. Piskorz, I. Komaromi, R. L. Martin, D. J. Fox, T. Keith, M. A. Al-Laham, C. Y. Peng, A. Nanayakkara, M. Challacombe, P. M. W. Gill, B. Johnson, W. Chen, M. W. Wong, C. Gonzalez, and J. A. Pople, Gaussian, Inc., Pittsburgh PA, 2003.

[28] H. Tachikawa, J. Phys. Chem. C, 115, 20406 (2011).

[29] H. Tachikawa and H. Kawabata, J. Phys. Chem. C, 113, 7603 (2009).

[30] H. Tachikawa, Y. Nagoya, and H. Kawabata, J. Chem. Theor. Comput. 5, 2101 (2009).

Figure captions

Figure 1. (color online). Optimized structure of alkyl radical-fullerene complexes (R-C_{60}) calculated at the CAM-B3LYP/6-311G(d,p) level. The values indicate the bond distance in A.

Figure 2. (color online). Potential energy curve (PEC) for the addition of butyl radical (n=4n) to C_{60}.

Figure 3. (color online). Optimized structures of R-C_{60} at transition state (TS). Bond lengths and angles are in A and in degrees, respectively.

Figure 4. (color online). Spatial distributions of spin densities on R(n=4)-C_{60} system at van der Waals (vdW) state, TS, and addition complex (PD) with the binding structure.

Figure 5. (color online). Simulated absorption spectra of C_{60} and C_{60}-R complexes (vdW and PD states).

Figure 6. (color online). Molecular orbitals contributing to the electronic excitations.

Figure 7. (color online) Potential energy diagrams of alkyl radical addition reaction to C_{60} surface. The values indicate relative energies (in kcal mol^{-1}) along the reaction coordinate.

Table 1. Binding energies (E_{bind} in kcal mol^{-1}) of alkyl radicals to C_{60}.

n	6-31G(d)	6-311G(d,p)
1	37.1	35.1
2	33.7	31.8
3	34.1	32.2
4n	34.0	32.1
4t	25.7	24.1

Table 2. Optimized geometrical parameters(R(C_0-C_1) in Å) and binding energies (E_{vdW} in kcal mol^{-1}) of vdW complexes, R—C_{60}. The calculation was carried out the CAM-B3LYP/6-311G(d,p) level.

n	R(C_0-C_1) / Å	E_{vdW} / kcal mol^{-1}
1	3.684	-0.4
2	3.667	-0.6
3	3.639	-0.6
4n	3.636	-0.5
4t	3.560	-0.8

Table 3. Activation energies (E_{act} in kcal mol^{-1}) of addition of alkyl radicals to C_{60}.

n	6-31G(d)	6-311G(d,p)
1	1.96	2.81
2	1.28	2.10
3	1.16	2.08
4n	1.23	2.12

Table 4. Coefficients of equation (2) obtained from the NBO analysis

n	a	b	m	l
1	0.706	0.708	2.83	2.02
2	0.709	0.705	2.86	1.95
3	0.710	0.705	2.87	1.95
4n	0.707	0.708	2.88	2.01
4t	0.705	0.710	2.90	1.99

Table 5. Hyperfine coupling constants (hfccs) of protons in the alkyl radicals along the reaction coordinate calculated at CAM-B3LYP/6-311G(d,p)

n	position	*alkyl* radical	vdW	TS	PD
1	H_1	-22.56	-23.04	-17.61	-0.06
2	H_1	-22.35	-22.09	-16.51	-0.98
	H_2	+26.03	+25.95	+19.41	+0.17
3	H_1	-22.13	-21.80	-16.44	-0.97
	H_2	+11.05	+10.85	+7.06	-0.08
	H_3	+0.70	+0.78	+1.29	+0.29
4	H_1	-22.13	-21.91	-16.44	-0.97
	H_2	+11.28	11.18	+7.21	-0.08
	H_3	-1.41	-1.40	-0.99	+0.07
	H_4	+0.16	0.15	+0.20	+0.02

Figure 1.

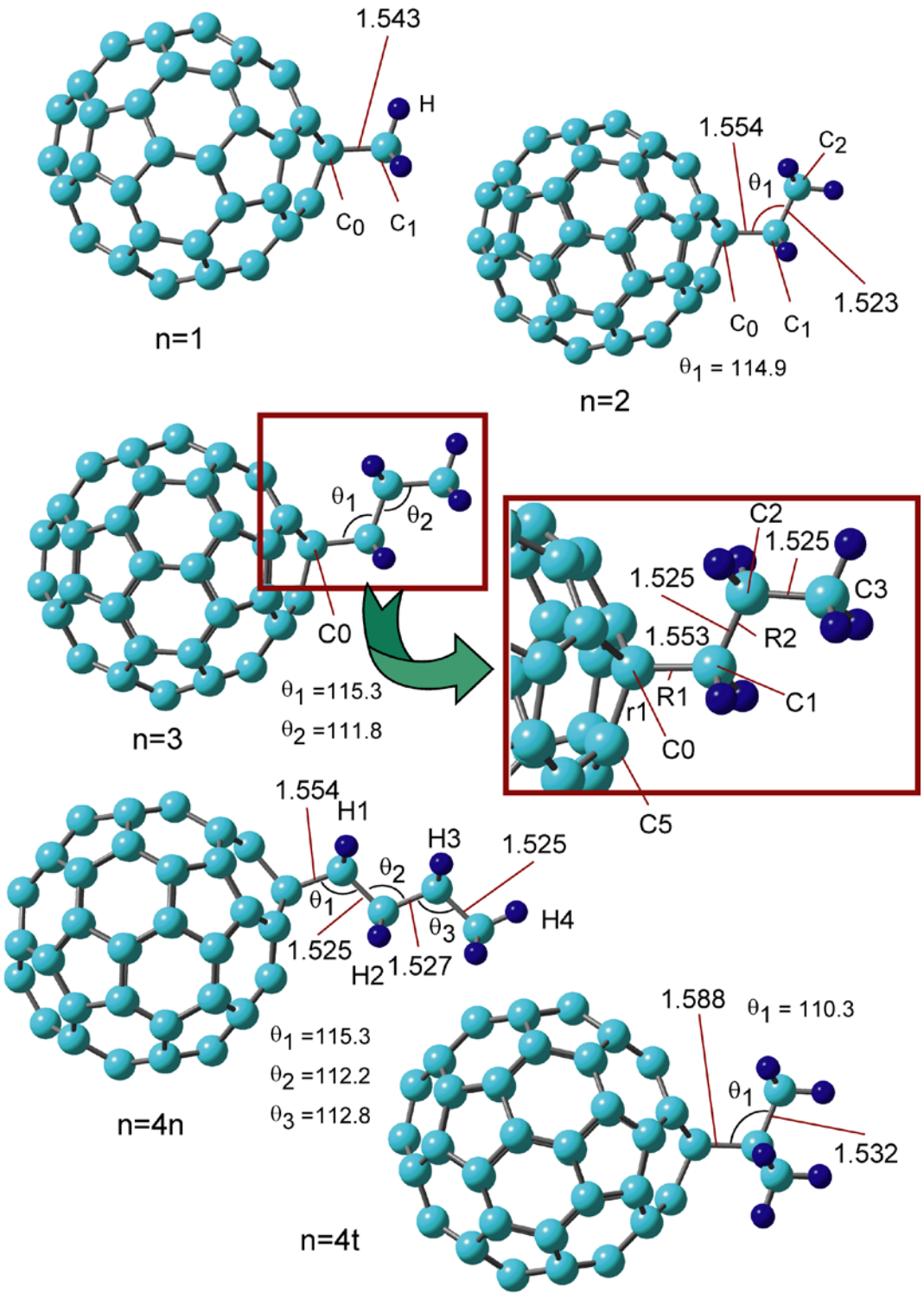
1.543
H
C0
C1
n=1
1.554
C2
θ1
1.523
C0
C1
θ1 = 114.9
n=2
θ1
θ2
C0
θ1 =115.3
θ2 =111.8
n=3
C2
1.525
1.525
C3
1.553
R2
R1
C1
r1
C0
C5
1.554
H1
H3
1.525
θ2
θ1
θ3
H4
1.525
H2
1.527
θ1 =115.3
θ2 =112.2
θ3 =112.8
n=4n
1.588
θ1 = 110.3
θ1
1.532
n=4t

Figure 2.

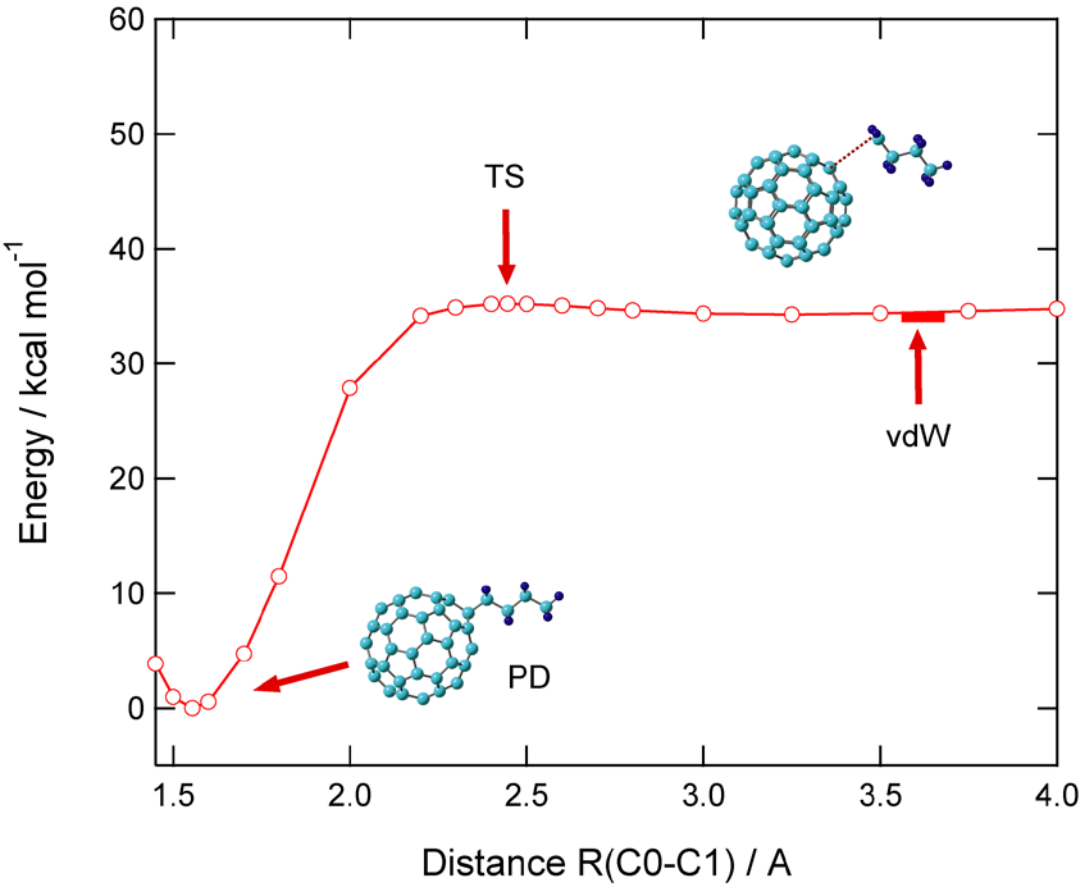
60
50
40
30
20
10
0
Energy / kcal mol-1
TS
vdW
PD
1.5
2.0
2.5
3.0
3.5
4.0
Distance R(C0-C1) / A

Figure 3.

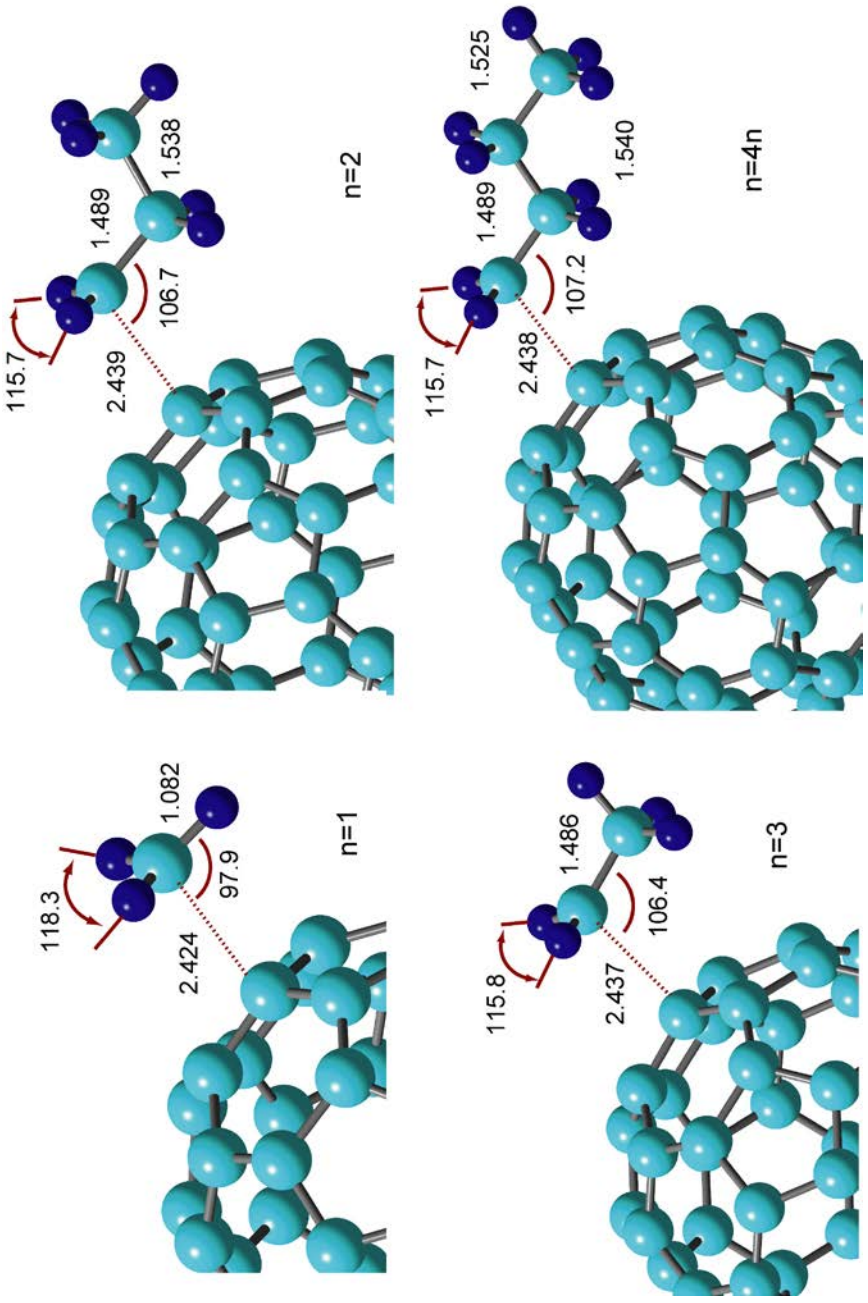
n=2
1.538
1.489
106.7
115.7
2.439
n=4n
1.525
1.540
1.489
107.2
115.7
2.438
n=1
1.082
97.9
118.3
2.424
n=3
1.486
106.4
115.8
2.437

Figure 4.

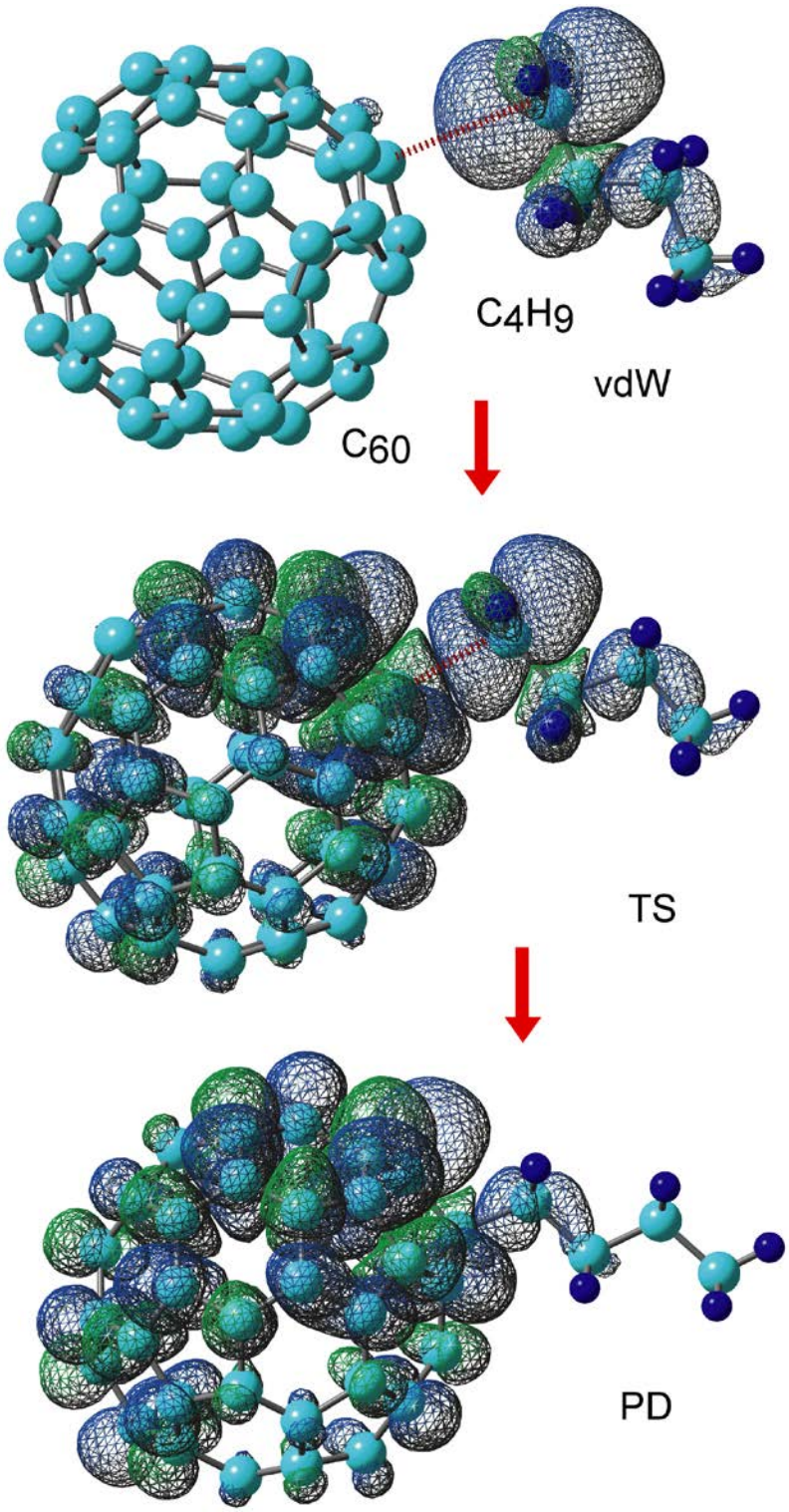

Figure 5.

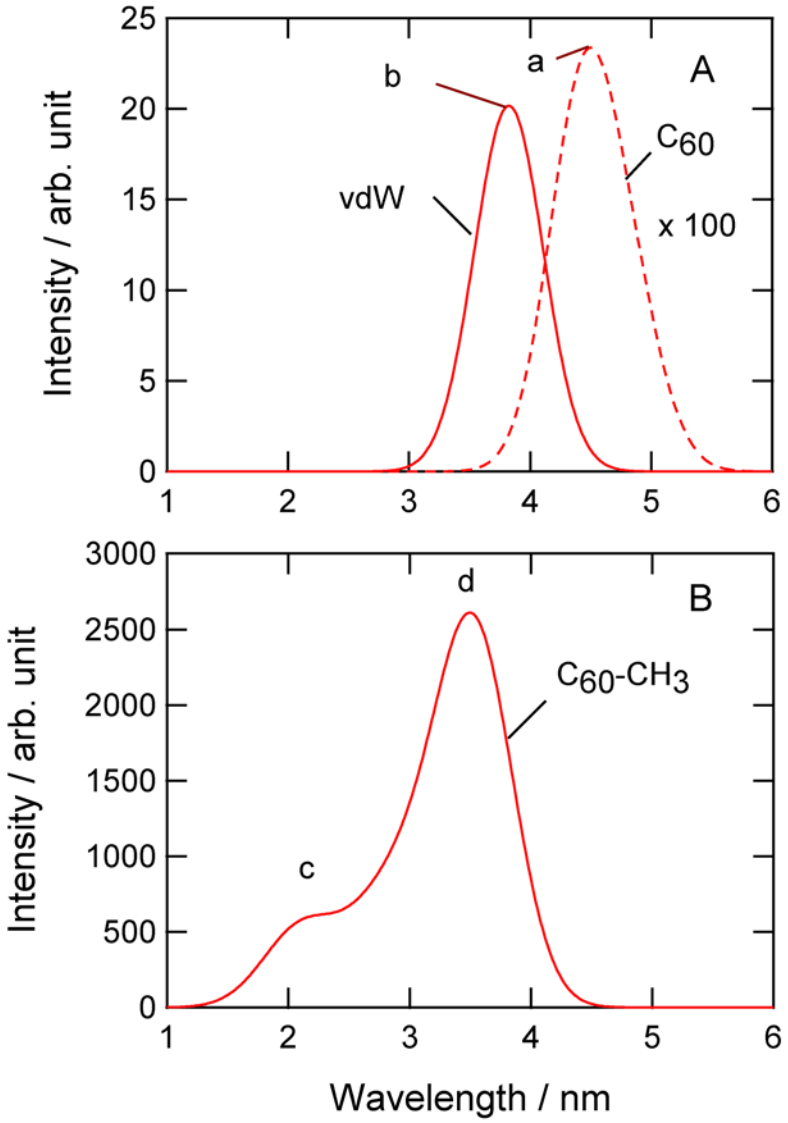
Intensity / arb. unit
25
20
15
10
5
0
1
2
3
4
5
6
a
b
A
C60
vdW
x 100
Intensity / arb. unit
3000
2500
2000
1500
1000
500
0
d
B
C60-CH3
c
Wavelength / nm

Figure 6.

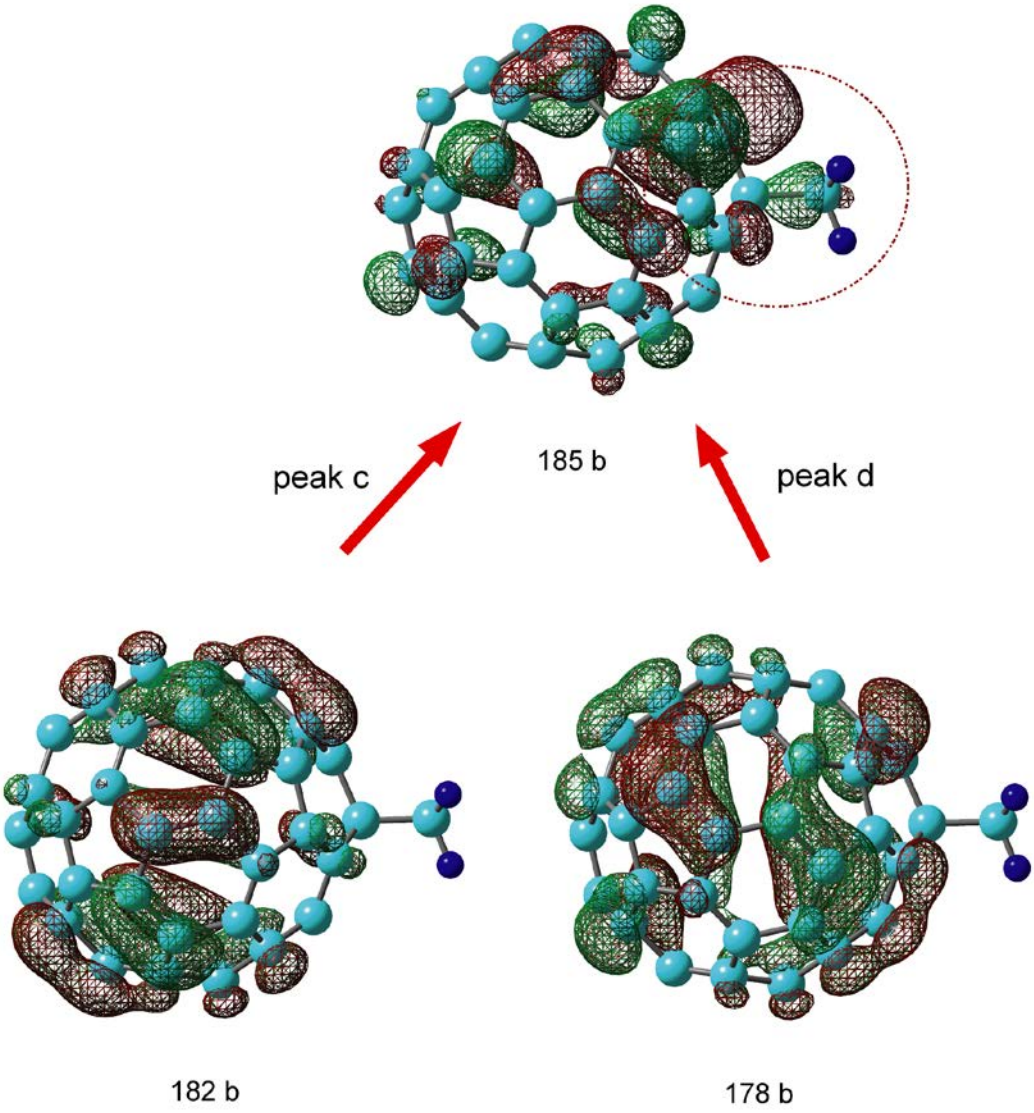

Figure 7.

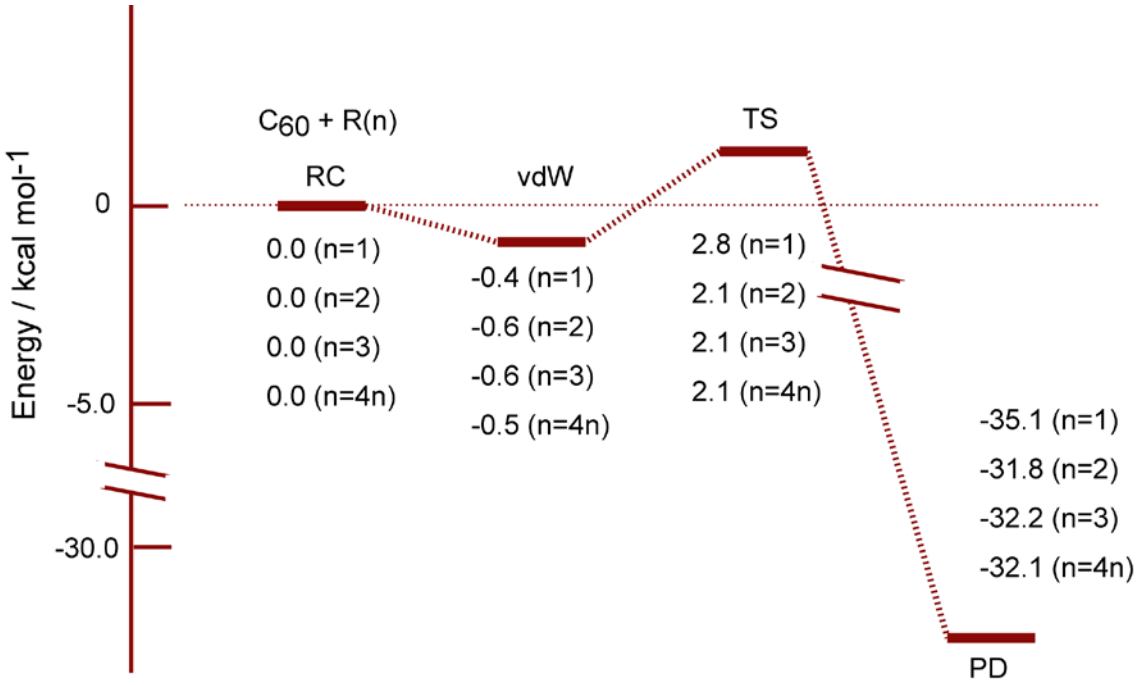
Energy / kcal mol-1
0
-5.0
-30.0
C60 + R(n)
RC
0.0 (n=1)
0.0 (n=2)
0.0 (n=3)
0.0 (n=4n)
vdW
-0.4 (n=1)
-0.6 (n=2)
-0.6 (n=3)
-0.5 (n=4n)
TS
2.8 (n=1)
2.1 (n=2)
2.1 (n=3)
2.1 (n=4n)
PD
-35.1 (n=1)
-31.8 (n=2)
-32.2 (n=3)
-32.1 (n=4n)